Potassium tune-out-wavelength measurement using atom interferometry and a multipass optical cavity

Raisa Trubko, Maxwell D. Gregoire, William F. Holmgren, and Alexander D. Cronin

Phys. Rev. A **95**, 052507 — Published 26 May 2017

DOI: 10.1103/PhysRevA.95.052507

Tune-Out Wavelength Measurement of Potassium with Atom Interferometry and a Multi-Pass Optical Cavity

Raisa Trubko[1], Maxwell D. Gregoire[2], William F. Holmgren[2], and Alexander D. Cronin[1,2]
College of Optical Sciences University of Arizona, Tucson, Arizona 85721, USA and
Department of Physics, University of Arizona, Tucson, Arizona 85721, USA
(Dated: April 28, 2017)

The longest tune-out wavelength for potassium atoms, $\lambda_{\rm zero} = 768.9701(4)$ nm, was measured using an atom interferometer with a large irradiance gradient supported in a multi-pass optical cavity. Systematic errors in $\lambda_{\rm zero}$ measurements that arise from laser light, Doppler shifts, and the Earth's rotation are described. The ratio of oscillator strengths for the potassium D2 and D1 lines inferred from this $\lambda_{\rm zero}$ measurement is $\rho = f_{\rm D2}/f_{\rm D1} = 2.0066(11)$, and the ratio of line strengths is $R = S_{\rm D2}/S_{\rm D1} = 1.9977(11)$.

Tune-out wavelengths ($\lambda_{\rm zero}$) are associated with roots in the dynamic polarizability spectrum of an atom. Light at a tune-out wavelength therefore causes zero energy shift (no ac-Stark shift) for atoms in a particular state. Precise $\lambda_{\rm zero}$ measurements [1–5] serve as a means to study several atomic properties including lifetimes, oscillator strengths, oscillator strength ratios, atomic scalar, vector, and tensor polarizabilities and hyperpolarizabilities, the polarization of atomic core electrons, core-valence electron correlations, and relativistic and QED effects on atomic transition amplitudes [6–15]. Improved knowledge of $\lambda_{\rm zero}$ values can also be important for several experiments that use species-specific and state-specific optical dipole potentials created with light near a tune-out wavelength [16–23]. Tune-out wavelengths, also known as magic-zero wavelengths, were mentioned in 2004 by Safronova, Williams and Clark [6]. They were introduced in more detail in 2007 by LeBlanc and Thywissen [16], and more precise calculations of several $\lambda_{\rm zero}$ were presented in 2011 by Arora, Safronova and Clark [7]. The most accurate measurements of tune-out wavelengths to date have used atom diffraction [1, 5], atom interferometry [2, 3], and studies of trapped atom dynamics [4].

Here we present an improved measurement of the longest tune-out wavelength for potassium, $\lambda_{\rm zero} = (786{,}970.14 \pm 0.42)$ pm. We describe how we made this measurement using a multi-pass optical cavity to recycle light shining on an atom interferometer. Then we discuss methods we used to reduce errors and estimate systematic uncertainties. Finally, we interpret this measurement in terms of the the ratio of line strengths

$$R = \frac{S_{\rm D2}}{S_{\rm D1}} = \frac{|\langle 4s\|D\|4p_{3/2}\rangle|^2}{|\langle 4s\|D\|4p_{1/2}\rangle|^2} = 1.9977(11) \qquad (1)$$

and the ratio of oscillator strengths

$$\rho = \frac{f_{\rm D2}}{f_{\rm D1}} = R\left(\frac{\omega_{\rm D2}}{\omega_{\rm D1}}\right) = 2.0066(11) \qquad (2)$$

for the D1 and D2 lines in potassium associated with the $4s$-$4p_{1/2}$ and $4s$-$4p_{3/2}$ transitions, and we discuss the impact of this measurement on our knowledge of the $4p_{1/2}$ and $4p_{3/2}$ state lifetimes.

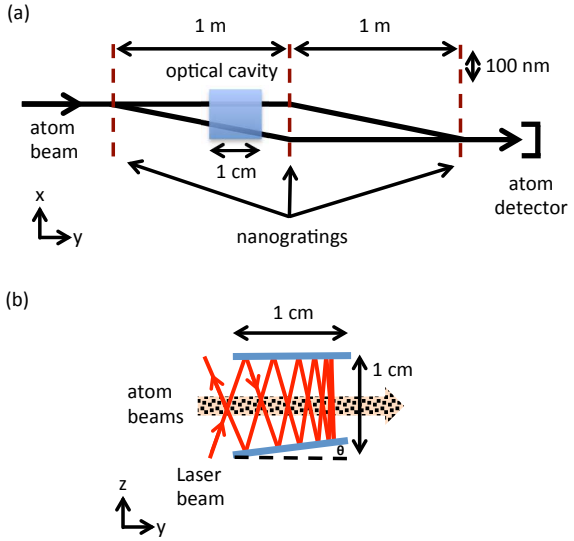

FIG. 1. (Color online) (a) Top-view schematic of atom interferometer paths passing through a multi-pass optical optical cavity. (b) Side-view schematic of the plane-plane optical multi-pass cavity aligned so atoms interact with multiple passes of the laser beam. The deviation from parallel is exaggerated to show how the laser beam folds back at different angles.

To measure $\lambda_{\rm zero}$ we applied an irradiance gradient on the paths of a three-nanograting Mach-Zehnder atom beam interferometer [24–26] as shown in Fig. 1. Then we report the root in the light-induced phase shift spectrum,

$$\phi(\omega) = \frac{\alpha(\omega)}{2c\hbar\epsilon_o v}\int s\frac{d}{dx}I\,(x,y;\omega)\;dy, \qquad (3)$$

where $\omega = 2\pi c/\lambda$ is the laser frequency, v is the atom beam velocity, s is the atom wave-packet separation, and dI/dx is the irradiance gradient. Figure 1 shows the coordinate axes.

A. Multi-Pass Cavity Enhancement

To improve the precision of $\lambda_{\rm zero}$ measurements we built an optical cavity that increases the line-integral of the irradiance gradient $\int \frac{dI}{dx} dy$. We used an optical fiber to guide light directly into the vacuum chamber and to launch a laser beam into a multi-pass optical cavity (MPC). The MPC is made of two plane mirrors separated by $\ell = 1$ cm. The mirrors surround the atom beam as sketched in Fig. 1 so atoms interact with approximately 40 passes of the laser beam. This is not a stable resonator (the laser spots walk and grow without bound), so we refer to it as a multi-pass cavity (MPC).

To quantify the benefit of the MPC we first discuss the phase shift $\phi_{\rm single}$ caused by a single laser beam propagating in $\hat{z}$ with an irradiance profile $I = [2P/(\pi w^2)] \exp[-2(x^2+y^2)/w^2]$ where P is the power and w is the beam width (radius at e^{-2} irradiance). From Eq. (3), the phase $\phi_{\rm single} \propto \int \frac{dI}{dx} dy = [8Px/(\sqrt{2\pi} w^3)] \exp[-2x^2/w^2]$ is maximized when the laser beam center is offset from the atom beam paths by $x = w/2$. Then, with that optimized alignment, $\phi_{\rm single} \propto \left| \int \frac{dI}{dx} dy \right|_{\rm max} = (8/e\pi)^{-1/2} \left(P/w^2\right)$. Because the laser beam width is large compared to the $s = 20\mu$m separation of the atom interferometer paths ($w \gg s$), we neglect higher order derivatives, e.g. $\frac{d^2}{dx^2} \int I dy$. We find the maximum phase shift due to a single pass of a laser beam is

$$\phi_{\rm single} = \left(\frac{2}{e\pi}\right)^{-1/2} \frac{\alpha(\omega) s}{c\hbar\epsilon_o v} \frac{P}{w^2} \tag{4}$$

Since $\phi_{\rm single}$ is proportional to P/w^2, we are motivated to use a smaller waist to get a bigger signal. However, the 60μm thickness of the atom beam sets a constraint on the minimum waist w. If the laser beam is smaller than this, it tends to reduce the ensemble- averaged light-induced phase shift and contrast. Therefore, we chose $w \approx 60$ μm to produce a more uniform irradiance gradient across all of the atom beam paths.

Fully separated interferometer paths would enable us to apply light on one path while leaving the other path through the interferometer completely in the dark, as demonstrated in [3]. This would cause a phase $\phi_1 = \alpha(\omega)/(2c\hbar\epsilon_o v) \int I(\omega) dy$ that is larger than the gradient-induced phase shift in Eq.(4) by the ratio $\phi_1/\phi_{\rm single} = (\sqrt{e}/2)(w/s)$. However, producing such well-separated atom beam paths requires improved collimation and/or larger diffraction angles, both of which reduce the atomic flux in our apparatus. An alternative method to increase ϕ without reducing atomic flux is to use more laser power or recycle the laser light.

That is why we constructed a multi-pass cavity (MPC) to recycle light and thus increase light-induced phase shifts. Because the MPC sketched in Fig. 1b is built with two plane mirrors, the laser beam diameter eventually grows as the laser propagates in the MPC. Therefore, one might expect that there is a tradeoff between a small waist or a long Raleigh range, but this is not the case. Even though a smaller waist causes a larger signal for a single pass of the laser beam, a long Raleigh range makes several passes contribute significantly to ϕ. These factors compensate as shown with Eqns. (5) and (6).

The MPC enhances the signal by the factor

$$\frac{\phi_{\rm multi}}{\phi_{\rm single}} = w_0^2 \sum_n \frac{R'^n}{[w'(z')]^2} \tag{5}$$

where R' is the reflectivity of the mirrors and $w'(z') = w'_0[1+(z'/z'_{\rm R})^2]^{1/2}$ is the laser beam width. $z' = n\ell$ after n reflections in the plane-plane cavity where ℓ is the separation between the two mirrors, and $n = 0$ corresponds to the laser beam waist location. The Raleigh range is $z'_{\rm R} = \pi w'^2_0/\lambda$. We use primes ($w'$, z', and R') to indicate quantities for the laser beam in the MPC.

For comparison, w_0 is the waist in a single-pass experiment. For high reflectivity mirrors ($R \approx 1$) and $z'_{\rm R} \gg \ell$, we approximate the sum in Eq. (5) with the integral $\int [w'(z')]^{-2} dz'/\ell$ to find the enhancement factor

$$\frac{\phi_{\rm multi}}{\phi_{\rm single}} = \pi \left(\frac{w_0}{w'_0}\right)^2 \left(\frac{z'_{\rm R}}{\ell}\right) = \pi^2 \frac{w_0^2}{\lambda \ell}. \tag{6}$$

The last form shows that the enhancement is independent of w'_0 and $z'_{\rm R}$. For our experiments with $w_0 = 60$ μm, $\lambda = 769$ nm, and ℓ=1.0 cm, Eq. (6) yields a calculated enhancement of $\aleph = 4.6$. With reflectivity $R' = 99.7\%$, Eq. (5) predicts $\aleph = 4.0$.

We experimentally verified that our MPC increased the signal slope as shown in Fig. 2. With the MPC, the

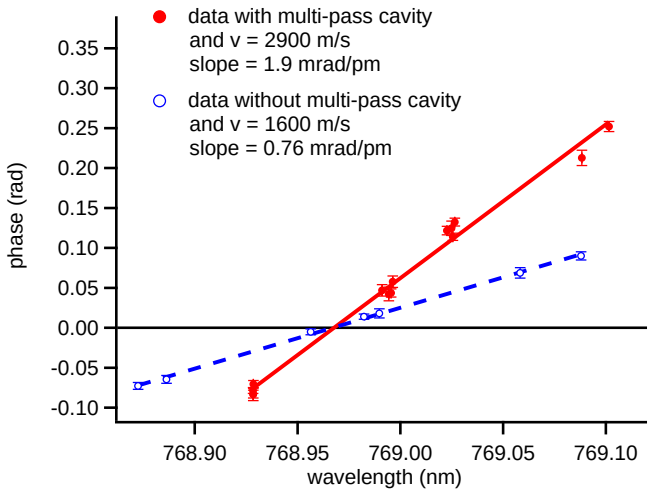

FIG. 2. (Color online) Enhanced slope for phase vs. wavelength data due to multi-pass cavity. The slope for $\phi_{\rm multi}$ is $d\phi/d\lambda = 1.9$ mrad/pm with $v = 2900$m/s atoms (solid line and solid circles). A smaller slope of 0.76 mrad/pm was observed for a single-pass experiment ($\phi_{\rm single}$) with $v = 1600$m/s atoms (dashed line and open circles).

slope of $d\phi/d\lambda$ = 1.9 mrad/pm with 2900 m/s potassium atoms was significantly larger than the slope $d\phi/d\lambda$ = 0.76 mrad/pm that we observed with a single pass of the laser beam. This was true even though we had used slower (1600 m/s) potassium atoms for the single pass experiments. For a more direct comparison, because the signal slope depends on v^{-2} we predict that a single-pass experiment with 2900 m/s potassium atoms in our experiment would have an even smaller slope of 0.23 mrad/pm. This predicted single-pass slope is 8.2 times smaller than the slope we observed with the MPC. This validates that the MPC is serving its purpose. The data with the MPC used for the tune-out wavelength measurement presented here were obtained over nine days with an average signal slope of 2.1 mrad/pm and an RMS distribution of 0.5 mrad/pm.

Our experiment also benefited from improved mechanical stability associated with the MPC and with bringing the laser into the atom interferometer vacuum chamber via an optical fiber. Repeated measurements of $\lambda_{\rm zero}$ demonstrated less scatter than we had in [2] by factor of 6. The MPC improved our statistical precision for $\lambda_{\rm zero}$ measurements from 1.4 pm in [2] to 0.3 pm in the present work. In each case we quote a 2σ statistical uncertainty (where σ is the standard error of the mean [27]), and both [2] and this measurement used approximately 30 hours of data.

Another example of an optical cavity to enhance irradiance on an atom interferometer was described by Hamilton *et al.* [28] who used intra-cavity light to make an atom interferometer. In comparison, we only used a cavity as an interaction region. Yet, similar to Hamilton *et al.*, we benefit from increased light-atom interactions intra-cavity. In principle, a resonant cavity with curved mirrors can further increase irradiance and maintain smaller beam waists in a cavity mode, both factors which would increase $d\phi/d\lambda$. Resonant cavities can also serve as a spectral filter, which can be both beneficial and detrimental as we discuss in the "Tuning-Out Broadband Light" section of this paper.

B. Choice of Atom Velocity

Experimentally, we found it more favorable to work with velocities of 2500 m/s as compared to 1600 m/s. So, here we discuss reasons why there may be an optimum atom beam velocity for $\lambda_{\rm zero}$ measurements with our apparatus. The velocity of the atoms has an effect on the signal to noise for two reasons. First, slower atoms receive larger light-induced phase shifts because the signal ϕ is proportional to v^{-2}. This is because the interaction time is proportional to $1/v$, and the separation, s in Eq. (3), depends on the de Broglie wavelength $\lambda_{dB} = h/mv$. However, slower atom beams also have much lower atom count rates ($N \propto v^3$), and therefore worse statistical precision (shot noise) in phase described by $\delta\phi = (C\sqrt{N})^{-1}$. Thus, the shot noise limited signal to noise ratio is

$$SNR = \frac{\phi}{\delta\phi} \propto \frac{C}{\sqrt{v}} \tag{7}$$

This naïve estimate shows that higher signal to noise ratios would be obtained with velocity as low as possible. However, this assumed zero detector background noise and zero drifts in the laser wavelength, laser power, laser beam alignment, and atom fringe reference phase over time.

If we consider a more realistic model with a flux-independent background (average) atom count rate due to detector noise, then we find there is an optimum atom beam velocity. If the observed counts $N = N_0 + B$ are the sum of N_0 detected atoms and B background counts, this increases the fluctuations in counts and reduces contrast so

$$C = C_0 \frac{N_0}{N_0 + B} \tag{8}$$

where C_0 is the contrast that would be observed if B=0. Then

$$\delta\phi = \frac{1}{C\sqrt{N}} = \frac{\sqrt{N_0 + B}}{C_0 N_0} \tag{9}$$

and

$$SNR = \frac{\phi}{\delta\phi} \propto \frac{v^{-2} C_0 N_0}{\sqrt{N_0 + B}} \tag{10}$$

Now let $N_0 = kv^3$, where $k = 100B/(3\text{km/s})^3$ is typical. This means that the background B is about 1% of the count rate that we observe with 3 km/s atom beams. Then we find the velocity that maximizes SNR is

$$v = \left(\frac{2B}{k}\right)^{1/3} = 814 \text{ m/s} \tag{11}$$

This model of signal to noise identifies a non-zero optimum velocity. Additional phase noise due to drifts in alignment will make the optimum velocity even higher. This is because faster atoms provide higher flux, and this enables us to operate experiments faster and thus control for drifts better. Hence, our selection of 2 to 3 km/s atoms may be close to optimal.

C. Decoherence Spectroscopy

The MPC causes a set of Doppler shifts. As indicated in Fig. 1 we do not have a simple crossed-beam experiment. Instead there are many laser beams crossing at different angles relative to the atom beam.

To measure the range of Doppler shifts in our multi-pass cavity we developed *decoherence spectroscopy* [29]. This technique uses quantum decoherence due to photon scattering to cause laser wavelength dependent contrast loss.

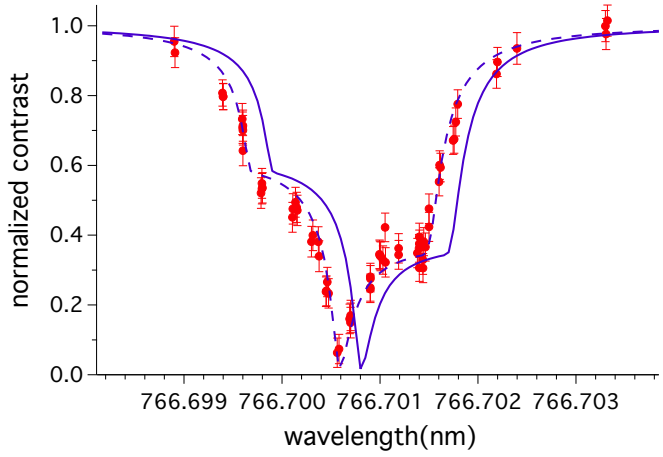

FIG. 3. (Color online) Decoherence spectroscopy data (red solid circles) showing contrast vs laser wavelength. Theoretical curves are shown in solid blue for no Doppler shift and dashed blue for a −0.21 pm Doppler shift. The best fit model indicates that a +0.21 pm shift should be added to our $\lambda_{\rm zero}$ measurements due to Doppler shifts in the MPC [29].

For decoherence spectroscopy we used the same experimental laser beam and atom beam geometry as we did for $\lambda_{\rm zero}$ measurements, but the laser wavelength is tuned near resonance (across the D2 line). The laser power is also attenuated by several orders of magnitude to reduce power broadening. Then, we monitor the atom interference fringe contrast as a function of laser wavelength as shown in Fig. 3.

A model decoherence spectrum shown as a dotted blue line in Fig. 3 makes the best fit to the decoherence data. The theory used for the fits to the data is explained in [29]. The measured contrast spectrum is shifted by (-0.21 ± 0.10) pm from the theoretical prediction. Therefore, we apply a (+0.21 ± 0.10) pm correction to our $\lambda_{\rm zero}$ measurement. This correction accounts for the net Doppler shift in our experiment and for any systematic errors of the Bristol 621B wavemeter that we use to measure the laser wavelength.

D. Tuning-Out Broadband Light

Broadband light from a tapered amplifier (TA) laser can cause errors in $\lambda_{\rm zero}$ measurements. Therefore, we measured the spectrum of broadband emission of our TA and controlled it in order to minimize systematic errors in $\lambda_{\rm zero}$.

For more background, as discussed by Bolpasi and von Klitzing [30], there are several categories of atomic physics experiments for which broadband light causes problems such as heating, decoherence, or background signals. There are also some types of experiments such as fluorescence spectroscopy and magneto optical trapping that are not adversely affected by a small amount of off-mode light. However, in experiments to measure $\lambda_{\rm zero}$, broadband light near a resonance can add significant light-induced phase shifts.

To minimize broadband light we saturate the TA (Eagleyard EYP-TPA-0765-02000) with 20 mW of light from an external cavity diode laser (Eagleyard EYP-RWE-0790-04000) after an optical isolator, and spatially filter the 1.2 W TA output by focusing it into a single mode optical fiber (Thorlabs SM-600) after another optical isolator. The fiber brings 200 mW of light into the multi-pass cavity in vacuum.

To measure the broadband spectrum shown in Fig. 4, we used a Photon Control model SPM-002-C grating spectrometer in conjunction with a thin (1 mm) glass étalon, which increases the effective dynamic range of the spectrometer. A dark fringe and bright fringe are used alternately to suppress or transmit the the monochromatic component of the laser. A dark fringe in reflection from the étalon suppresses the monochromatic component of the laser by a factor of 1000, whereas, the broadband light spectrum is spread over many étalon fringes. Étalon fringes are not resolved in Fig. 4 since the 0.2 nm (100 GHz) free spectral range of the étalon is five times smaller than the 1 nm resolution of the grating spectrometer. Thus, the power of the broadband light spectrum is two times larger than what is measured and we make a correction for this effect. Suppressing the monochromatic light increased the dynamic range of our spectrometer system sufficiently for us to measure the broadband spectrum when the TA was seeded. For comparison, the unseeded TA light has about three times more power and a 1 to 2 nm bluer broadband spectrum (not shown). We observed the broadband spectrum shown in Fig. 4 using a

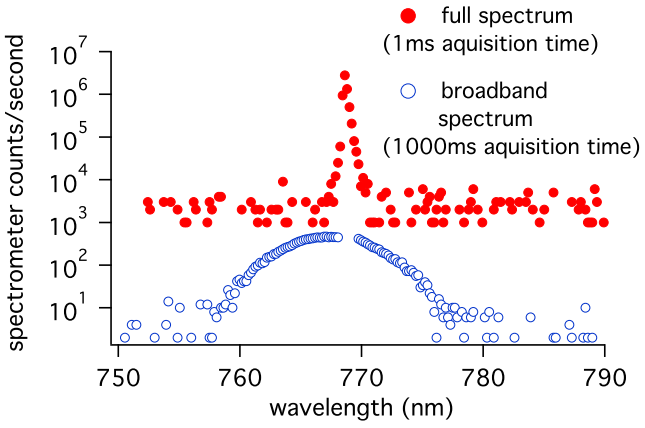

FIG. 4. (Color online) Power spectrum output from our tapered amplifier. The broadband spectrum (open blue circles) was observed with 1000 times more acquisition time while using a dark fringe from an étalon to suppress the monochromatic component of the spectrum, as described in this paper. A spectrum with the monochromatic light tuned to a bright fringe of the étalon is shown with a solid red circles.

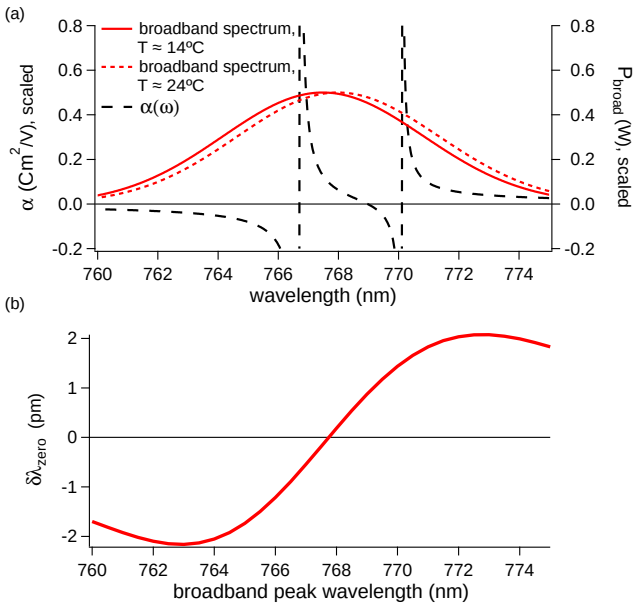

FIG. 5. (Color online) Error in $\lambda_{\rm zero}$ due to broadband light. (a) Spectra of $\alpha(\omega)$ and $P_{\rm broad}$ vs. wavelength used in Eq. (14) to calculate $\phi_{\rm BB}$. Two different $P_{\rm broad}$ spectra indicate how temperature-tuning the tapered amplifier laser adjusts the peak wavelength $\lambda_{\rm BB}$ of the broadband light. $P_{\rm broad}$ and $\alpha(\omega)$ are scaled in order to be viewed conveniently on the same graph. (b) Resulting error ($\delta\lambda_{\rm zero}$) as a function of the broadband peak wavelength $\lambda_{\rm BB}$.

500 ms acquisition time. We measured the relative power in the monochromatic peak using a maximum in reflection from the étalon (a bright fringe) and reducing the spectrometer acquisition time to 0.5 ms. The asymmetric spectral peak reported for the monochromatic light in Fig. 4 is due to the spectrometer's response, as we verified using a monochromatic HeNe laser.

Scanning the seed laser wavelength by 1 nm causes no observed changes in the broadband spectrum of the laser. This is important because to measure $\phi(\lambda)$ we scan the wavelength of the seed laser on either side of $\lambda_{\rm zero}$ as shown in Fig. 2. Also of note, the peak wavelength of the broadband spectral component depends on the temperature of the TA's water-cooled mount. With this, we can minimize shifts in $\phi(\lambda)$ caused by broadband light by adjusting the TA temperature.

To model how broadband light affects our $\lambda_{\rm zero}$ measurement, we write the TA output spectrum as a monochromatic component plus a broadband component:

$$P_{\rm laser}(\lambda) = P_{\rm mono}(\lambda) + P_{\rm broad}(\lambda). \tag{12}$$

A delta-function spectrum describes the amplified monochromatic laser light, $P_{\rm mono}(\lambda) = P_M\delta(\lambda - \lambda_{\rm M})$, where $P_{\rm M}$ is the power of the monochromatic component and $\lambda_{\rm M}$ is the wavelength of the monochromatic component. A Gaussian distribution describes the broadband component, $P_{\rm broad}(\lambda) = P_{\rm BB}(\sigma_{\rm BB}\sqrt{2\pi})^{-1}\exp[-(\lambda - \lambda_{\rm BB})^2/(2\sigma_{\rm BB}^2)]$, where $P_{\rm BB}$ is the power of the broadband component, $\lambda_{\rm BB}$ is the peak wavelength of the broadband distribution, and $\sigma_{\rm BB}$ is the RMS width of the Gaussian broadband distribution. This representation leads to a two-component model of the phase shift

$$\phi_{\rm total}(\lambda_{\rm M}) = \phi(\lambda_{\rm M}) + \phi_{BB} \tag{13}$$

where $\phi(\lambda_{\rm M})$ is given by Eq. (3) with $\omega = 2\pi c/\lambda_{\rm M}$, and and the phase shift due to the broadband radiation from the seeded TA is

$$\phi_{BB} = \frac{1}{2\epsilon_o c\hbar v}\int\int s\,\alpha(\omega)\frac{dI_{\rm broad}(\omega;x,y)}{dx}dy\,d\omega \tag{14}$$

with the spectrum of $I_{\rm broad}(\omega;x,y)$ found from the measured $P_{\rm broad}(\lambda)$. Then the shift in measured $\lambda_{\rm zero}$ caused by ϕ_{BB} is

$$\delta\lambda_{\rm zero} = \phi_{\rm BB}\left(\frac{d\phi}{d\lambda}\right)^{-1}. \tag{15}$$

As shown in Fig. 5, the shift $\delta\lambda_{\rm zero}$ is an antisymmetric function of $\lambda_{\rm BB}$. Therefore we can tune the broadband spectrum to make $\delta\lambda_{\rm zero} = 0$.

If the spectral width of the broadband radiation is larger than the fine structure splitting, $\sigma_{BB} > \Delta\lambda_{\rm FS}$, then a peak wavelength $\lambda_{\rm BB}$ near

$$\lambda_{\rm BB,zero} \approx \lambda_{\rm D2} + \frac{f_{\rm D1}}{f_{\rm D1}+f_{\rm D2}}\Delta\lambda_{\rm FS} \tag{16}$$

can null $\phi_{\rm BB}$ and thus minimize error in $\lambda_{\rm zero}$. This $\lambda_{\rm BB,zero}$ is the peak wavelength for a broadband spectral component that causes zero phase shift. So we call $\lambda_{\rm BB,zero}$ the *broadband tune-out wavelength*. Here, the fine structure splitting is denoted by $\Delta\lambda_{\rm FS} \equiv \lambda_{\rm D1} - \lambda_{\rm D2}$, and for K, $\Delta\lambda_{\rm FS} = 3.4$ nm. To derive Eq. (16) we express dynamic polarizability as a sum-over-states with just the D1 and D2 excitations, we ignore α_r in Eq. (17), and we make the near-resonance approximation that $\omega_{\rm D1}^2 - \omega^2 \approx 2\omega(\omega_{\rm D1} - \omega)$. Hence $\lambda_{\rm BB,zero}$ is approximate, but it is significantly different than $\lambda_{\rm zero}$. For alkali atoms with an oscillator strength ratio [see Eq. (2)] of $\rho \approx 2$ we find the broadband tune-out wavelength is approximately $\lambda_{\rm BB,zero} = \lambda_{\rm D2} + (1/3)\Delta\lambda_{\rm FS}$, whereas the tune-out wavelength for monochromatic light is approximately $\lambda_{\rm zero} = \lambda_{\rm D2} + (2/3)\Delta\lambda_{\rm FS}$. For narrower broadband spectra (so the inequality $\sigma_{\rm BB} > \lambda_{\rm FS}$ is no longer satisfied) the peak wavelength that minimizes $\phi_{\rm BB}$ will shift from $\lambda_{\rm BB,zero}$ towards $\lambda_{\rm zero}$.

We controlled $\lambda_{\rm BBpeak}$ by adjusting the temperature of the tapered amplifier laser (to 14°C) with the goal of making $\lambda_{\rm BB} = \lambda_{\rm BB,zero}$. We used the spectrometer and étalon system to measure $\lambda_{\rm BB} = 767.5(3)$ nm, and $\sigma_{\rm BB} = 5(1)$ nm, and $P_{\rm M}/P_{\rm BB} = 370(40)$. With these data we used Eqs. (14) and (15) to infer that broadband light caused a systematic error of -0.08(8) pm for our tune-out wavelength measurement. Therefore, we applied a

correction of +0.08(8) pm before we present our final result for $\lambda_{\rm zero}$. This correction and the uncertainty in this correction are smaller than the statistical precision of our $\lambda_{\rm zero}$ measurement.

E. Minimizing Errors Due To Earth's Rotation

In Trubko *et al.* [22], we reported large (±200 pm) systematic shifts in measured tune-out wavelengths, $\lambda_{\rm zero,lab}$, due to the Earth's rotation rate, Ω_E, and elliptically polarized light. Such errors stem from balancing the Coriolis force with atomic-spin-dependent forces that are caused by light near a tune-out wavelength. In [22] we demonstrated that $\lambda_{\rm zero,lab}$ is more sensitive to Ω_E when we use circularly polarized light, magnetic fields parallel to the light propagation (along $\hat{z}$), and atom beams with broad velocity distributions. For the new $\lambda_{\rm zero}$ measurement reported here we reduced the sensitivity to Ω_E by using linearly polarized light, a transverse magnetic field (along $\hat{x}$), and a narrow atom beam velocity distribution. To create those conditions in the lab we installed a polarizer immediately prior to the MPC inside the vacuum system, we applied a 10 Gauss transverse magnetic field with coils outside vacuum, and we used a 50 μm diameter nozzle for the supersonic beam jet to obtain an RMS velocity spread of $\sigma_v = v_0/16$, where $v_0 = 2.9$ km/s is the most probable atomic velocity in the beam.

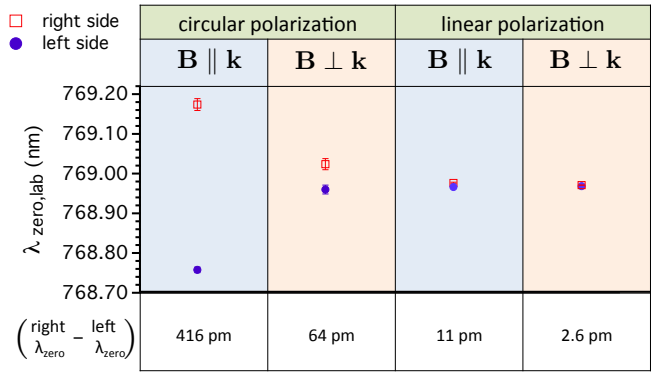

FIG. 6. (Color online) $\lambda_{\rm zero}$ measurement as a function of optical polarization and magnetic field orientation. Data with circularly polarized laser light are from [22] and were taken with $v \approx 1600$ m/s atom beams. Data with linearly polarized light were take with $v \approx 2900$ m/s atom beams. Open square red data show measurements with the laser beam on the right side of the interferometer and solid circle blue data show measurements on the left side.

To monitor systematic errors due to Ω_E we measured how the root $\lambda_{\rm zero,lab}$ depends on the sign of the irradiance gradient. Alternately illuminating the left and right sides of the atom interferometer reverses the sign of the atomic spin states (m_F numbers) that participate in phase echoes [22]. This changes the sign for the error $(\lambda_{\rm zero,lab} - \lambda_{\rm zero})$. Fig. 6 summarizes how the difference $\lambda^{\rm right}_{\rm zero,lab} - \lambda^{\rm left}_{\rm zero,lab}$ was reduced by using linearly polarized light and the transverse magnetic field. We attribute the remaining difference to smaller but still nonzero spin-dependent forces that change with the irradiance gradient. Therefore, as suggested by Trubko *et al.* [22] we report the average $\frac{1}{2}(\lambda^{\rm right}_{\rm zero,lab} + \lambda^{\rm left}_{\rm zero,lab})$ for our measurement of $\lambda_{\rm zero}$, as shown in Fig. 7. We estimate an additional systematic uncertainty of $(\lambda^{\rm right}_{\rm zero,lab} - \lambda^{\rm left}_{\rm zero,lab})/10 = 0.26$ pm associated with this averaging procedure. This uncertainty accounts for the fact that the magnitude and uniformity of the irradiance gradient, and hence the size of the systematic shift, can be slightly different when we reverse the sign of the irradiance gradient by moving the MPC from left to right.

I. RESULTS

Here we summerize the data acquisition, analysis, and error budget. Data in Fig. 8 were acquired with light chopped on or off in between every file. Each file index (point) represents 5 seconds of data. The wavelength of light was automatically switched every 125 seconds, and the laser wavelength was measured with a Bristol Instruments 621B wavemeter and recorded four times per second. Files with laser wavelength changes greater than 0.1 pm were ignored. The light-off data were used to remove the (∼6 rad/hr) phase drift. Twenty minutes of data from a series of 220 files shown in Fig. 8(a) were used to make $\phi(\lambda)$ spectra shown in Fig. 8(b). We obtain a $\lambda_{\rm zero}$ measurement from this spectrum by finding the root of a $\phi(\lambda)$ fit. The fitting procedure uses chi-

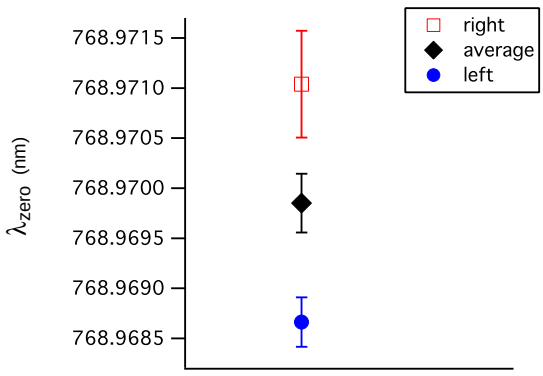

FIG. 7. (Color online) Determination of $\lambda_{\rm zero}$ from the average of average $\frac{1}{2}(\lambda^{\rm right}_{\rm zero,lab} + \lambda^{\rm left}_{\rm zero,lab})$. Only statistical error bars of 2 times the standard error of the mean are shown. Systematic corrections totaling 0.3 pm, and systematic uncertainties totaling 0.3 pm are later added before a final result is presented for $\lambda_{\rm zero}$.

squared minimization and a theoretical spectrum given by Eq. (3), where $\phi(\omega)$ is simplified to $\phi(\omega) = b\alpha(\omega)$ and $\alpha(\omega)$ is shown in Eqs. (17) and (18). R and b are the free parameters. This analysis is further described in [2]. Ninety-one data sets similar to Fig. 8, some longer in duration than others, representing over 30 hours of data in total, were compiled on a total of 9 different days to make 91 separate $\lambda_{\rm zero}$ measurements.

We compared results using the mean of all the data, the trimmed mean using the central 80% of the data, the weighted average using error bars that come from finding roots of individual $\phi(\lambda)$ data sets, and the trimmed weighted mean [27]. The results were all within 0.3 pm, and the statistical uncertainty (SEM) using these different methods ranged from 0.15 to 0.24 pm. For the final result we used the trimmed weighted means for $\lambda^{\rm right}_{\rm zero,lab}$ and $\lambda^{\rm left}_{\rm zero,lab}$ shown in Fig. 6.

The error budget for this $\lambda_{\rm zero}$ measurement is presented in Table I. The statistical uncertainty in $\lambda_{\rm zero}$ that we report, 0.3 pm, is twice the standard error of the mean [27]. Table I also summarizes the three types of systematic errors we discussed in the Sections on Decoherence Spectroscopy, Tuning-Out Broadband Light, and Minimizing Errors Due To Ω_E. These errors in turn are related to Doppler shifts, broadband light, and optical polarization. Table I summarizes the correction (if any) and the uncertainty due to each source. Our final result with corrections applied and statistical and systematic uncertainties added in quadrature is $\lambda_{\rm zero} = 768.9701(4)$ nm.

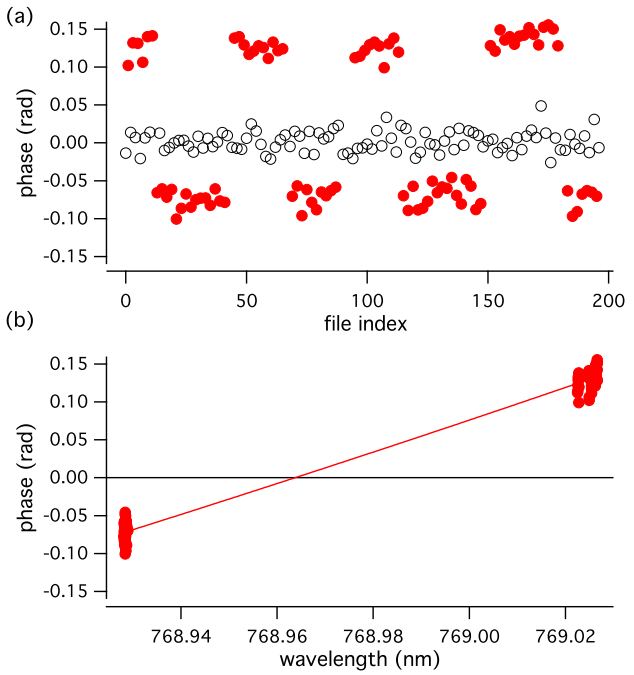

FIG. 8. (Color online) (a) Phase data for the laser shining on the right path of the interferometer. Each file contains five seconds of data. Laser light from the tapered amplifier was chopped on or off in between every file. Light-on data are shown in solid red circles, light-off data are shown in open black circles. After 24 files the seed laser wavelength was automatically changed. (b) Phase data from (a) versus laser wavelength. Corrections for the net Doppler shift and broadband laser light have not been applied to the shown data in (a) and (b).

TABLE I. Error budget for the $\lambda_{\rm zero}$ measurement. Statistical and systematic uncertainties added in quadrature combine to make the total uncertainty of 0.4 pm. Corrections due to known systematic shifts are also shown. The left/right shift refers to the error from the difference in $\lambda_{\rm zero}$ measurements when the irradiance gradient is greater on either the left or right arms of the atom interferometer, as shown in Figs. 6 and 7. The left/right shift depends on the optical polarization, the magnetic field orientation, the earth's rotation rate, and the atom beam velocity distribution, as described in this paper and in [22].

Source of error	Correction (pm)	Uncertainty (pm)
2 × Standard error of the mean	-	0.29
Doppler shift	+ 0.21	0.10
Broadband light	+ 0.08	0.08
Left/Right shift	-	0.26
Total	+ 0.29	0.41

II. DISCUSSION

Several calculations of tune-out wavelengths [7–14, 16] use the sum-over-states approach to calculate the dynamic polarizability $\alpha(\omega)$, expressed in terms of reduced dipole matrix elements $\langle i\|D\|k\rangle$ or oscillator strengths f_{ik}. For K between the D1 and D2 lines,

$$\alpha(\omega) = \frac{e^2 f_{D1}}{m\left(\omega_{D1}^2 - \omega^2\right)} + \frac{e^2 f_{D2}}{m\left(\omega_{D2}^2 - \omega^2\right)} + \alpha_{\rm r}$$

$$= \frac{\omega_{D1}\left|\left\langle 4s_{1/2}\right\|D\left\|4p_{1/2}\right\rangle\right|^2}{3\hbar\left(\omega_{D1}^2 - \omega^2\right)} + \frac{\omega_{D2}\left|\left\langle 4s_{1/2}\right\|D\left\|4p_{3/2}\right\rangle\right|^2}{3\hbar\left(\omega_{D2}^2 - \omega^2\right)} + \alpha_{\rm r} \tag{17}$$

where ω_{D1} and ω_{D2} are atomic resonance frequencies, and $\alpha_{\rm r} = \alpha_{\rm tail} + \alpha_{\rm core} + \alpha_{\rm vc}$ includes residual contributions from all transitions except the principle D1 and D2 transitions, contribution from core electrons, and the contribution from valence-core coupling [12, 31–34]. Theoretical values for α_r have been calculated by several theorists including [12, 31, 35]. Using our $\lambda_{\rm zero}$ measurement of 768.9701(4) nm and the theoretical $\alpha_r(\lambda_{\rm zero}) = 6.7009$ a.u.[12], we report the ratio of D1 and D2 line strengths for K as

$$R = \frac{S_{\rm D2}}{S_{\rm D1}} = \frac{|\langle 4s\|D\|4p_{3/2}\rangle|^2}{|\langle 4s\|D\|4p_{1/2}\rangle|^2} = 1.9977(11) \tag{18}$$

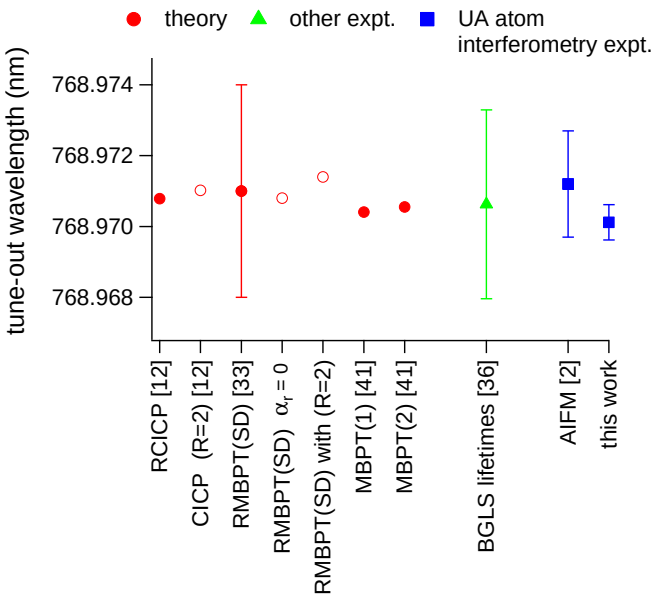

FIG. 9. (Color online) Comparison of measured and calculated values for the longest $\lambda_{\rm zero}$ for potassium. Calculations are shown in solid red circles. Calculations that assume $R = 2$ or $\alpha_r = 0$ are shown with open red circles. The result from lifetime measurements is shown with solid green triangles. Measurements made with atom interferometery are shown with solid blue squares.

and the ratio of oscillator strengths

$$\rho = \frac{f_{\rm D2}}{f_{\rm D1}} = R\left(\frac{\omega_{\rm D2}}{\omega_{\rm D1}}\right) = 2.0066(11) \qquad (19)$$

and the ratios of lifetimes

$$\frac{\tau_{4p_{1/2}}}{\tau_{4p_{3/2}}} = \frac{R}{2}\left(\frac{\omega_{D2}}{\omega_{D1}}\right)^3 = 1.01223(55). \qquad (20)$$

Independent measurements of state lifetimes by Volz *et al.* [36] established the value R= 1.9989(74). Holmgren *et al.* [2] found $R = 2.0005(40)$ based on a tune-out wavelength measurement. Now, with a more precise $\lambda_{\rm zero}$ measurement we report R=1.9977(11). Our new result has 6.7 has times smaller uncertainty for R than was experimentally measured without tune-out wavelengths. The uncertainty of 0.0011 for R reported here primarily comes from uncertainty in the measured $\lambda_{\rm zero}$. For comparison, a contribution of 0.0001 to the uncertainty in R is due to a 5% uncertainty in $\alpha_{\rm core}$. Our experiments with a multi-pass cavity have improved the statistical precision in the $\lambda_{\rm zero}$ measurement by a factor of 6 compared to [2]. However, due to the systematic shifts that we have described, the experiment with a multi-pass cavity has only improved the total uncertainty for R by a factor of 3.6 as compared to [2].

If we combine this new measurement of $\lambda_{\rm zero}$ with our recent measurement of static polarizability for potassium of $\alpha(0) = 289.7(3)$ a.u. [37, 38] and the theoretical value $\alpha_r(0) = 6.26(33)$ a.u.[31], then we can report the values for individual oscillator strengths, dipole matrix elements, lifetimes, and line strengths with reduced uncertainty. All of these physical quantities are related as described in [38]. For lifetimes of the $4p_{1/2}$ and $4p_{3/2}$ states, we report $\tau_{4p_{1/2}} = 26.78(4)$ ns and $\tau_{4p_{3/2}} = 26.46(4)$ ns. As a comparison, Volz *et al.* report independent lifetimes measurements $\tau_{4p_{1/2}} = 26.79(7)$ ns and $\tau_{4p_{3/2}} = 26.45(7)$ ns [36]. These results are consistent, but ours offer a smaller uncertainty. Other experiments by Wang *et al.* and Falke *et al.* are sensitive to the average of lifetimes, but not the difference (or ratio) of the the $\tau_{4p_{1/2}}$ and $\tau_{4p_{1/2}}$ lifetimes [39, 40].

Figure 9 compares calculations and measurements for the longest tune-out wavelength for potassium. We show experimental results in Fig. 9 from this work, from Holmgren *et al.* [2], and the $\lambda_{\rm zero}$ inferred from the independent measurements of the $4p_{3/2}$ and $4p_{1/2}$ state lifetimes by Volz *et al.* [36]. The only calculation with a published uncertainty so far is by Arora *et al.* [7], who presented $\lambda_{\rm zero}$= 768.971 nm with a 3 pm uncertainty based on many body perturbation theory (MBPT) calculations. Relativistic configuration interaction with core polarization (RCICP) calculations by Jiang *et al.* [12] showed $\lambda_{\rm zero}$ = 768.97077 nm. We also used results for dipole matrix elements from Johnson *et al.* [41, 42], which were already discussed in the context of R by [43], in order to infer $\lambda_{\rm zero}$ using Eq. (17).

Along with the theoretical results [7, 9, 41, 42] we plot shifted $\lambda_{\rm zero}$ values that show how the value of $\lambda_{\rm zero}$ from Aurora *et al.* would change if we assume a value of zero for α_r in Eq. (17). Setting $\alpha_r = 0$ decreases $\lambda_{\rm zero}$ by only 0.2 pm [12]. Then we show a shifted prediction for $\lambda_{\rm zero}$ that we produced using Eq. (17) and the hypothesis that $R = 2$ (but still using the measured values for $\lambda_{\rm D1}$ and $\lambda_{\rm D2}$). Setting $R = 2$ increases $\lambda_{\rm zero}$ by 0.4 pm.

Historical discussions of the oscillator strength ratio anomaly problem [33, 46–58] explain why R and ρ deviate from the statistical value of 2 that would be naïvely expected from the statistical degeneracies of the $4p_{3/2}$ and $4p_{1/2}$ states. Both relativistic effects and core polarization effects are important, as pointed out by Fermi in 1930 [59] and discussed extensively by Migdalek [46–48, 60–64]. Figure 10 shows theoretical predictions and experimental measurements for R and ρ for Na, K, Rb, and Cs. This shows that $R < 2$ and $\rho > 2$ are trends that get more pronounced for heavier atoms. With the $\lambda_{\rm zero}$ measurement presented in this work, we have shown that $R < 2$ with 2σ significance and $\rho > 2$ with 5σ significance for K atoms, where σ here refers to the total uncertainty in our $\lambda_{\rm zero}$ measurement summarized in Table I. To our knowledge, the $\lambda_{\rm zero}$ measurement presented here constitutes the first significant demonstration of the oscillator strength ratio anomaly for potassium.

To conclude, $\lambda_{\rm zero}$ measurements have stimulated creative experimental work in several laboratories, such as synchronized pulsing of light on atoms in a TOP trap

so as to control $\vec{k} \cdot \vec{B}$ [3], coherent addition of diffraction amplitudes from multiple short light pulses [1], and novel studies of atom trap dynamics [4]. In the work presented here, we developed a multi-pass cavity interaction region for an atom interferometer. We developed decoherence spectroscopy. We also used the concept of a broadband tune-out wavelength. These new methods help to improve $\lambda_{\rm zero}$ measurements and demonstrate new techniques for atom interferometry.

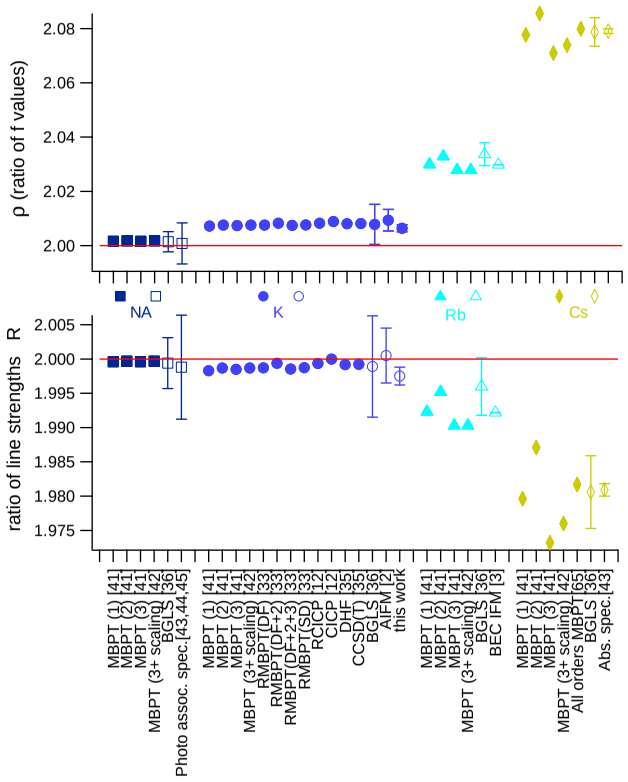

FIG. 10. (Color online) Theoretical calculations shown with solid circles, and experimental measurements shown with open circles, of ρ the ratio of oscillator strengths (top) and R the ratio of line strengths (bottom). MBPT refers to many-body perturbation theory and the number in parenthesis refers to the order [41]. RMBPT refers to relativistic many-body perturbation theory [33]. DF refers to Dirac-Fock basis orbitals [33]. SD refers to the single-double all order method [33]. RCICP refers to the relativistic configuration interaction plus core polarization approach [12]. CICP refers to the configuration interaction plus core polarization method [12]. DHF refers to the Dirac-Hartree-Fock method [35]. CCSD refers to singles-doubles coupled-cluster method [35]. BGLS refers to beam-gas-laser spectroscopy measurements [36]. AIFM refers to atom interferometry measurements. BEC IFM refers to interferometry measurements made with Bose-Einstein Condensates [3]. Photo assoc. spec. refers to Photo association spectroscopy [43–45]. Abs. spec. refers to Absorption Spectroscopy [43].

A. Acknowledgments

We thank Jaggar D. Henzerling and Matthew J. Lichtenberger for discussing systematic error analysis. This work is supported by NSF Grant No. 1306308 and a NIST PMG. R.T. and M.D.G thank NSF GRFP Grant No. DGE-1143953 for support.

[65]

[1] C. D. Herold, V. D. Vaidya, X. Li, S. L. Rolston, J. V. Porto, and M. S. Safronova, "Precision measurement of transition matrix elements via light shift cancellation,"

Phys. Rev. Lett. **109**, 243003 (2012).
[2] William F. Holmgren, Raisa Trubko, Ivan Hromada, and Alexander D. Cronin, "Measurement of a wavelength of light for which the energy shift for an atom vanishes," Phys. Rev. Lett. **109**, 243004 (2012).
[3] R. H. Leonard, A. J. Fallon, C. A. Sackett, and M. S. Safronova, "High-precision measurements of the ^{87}Rb D-line tune-out wavelength," Phys. Rev. A **92**, 052501 (2015).
[4] B. M. Henson, R. I. Khakimov, R. G. Dall, K. G. H. Baldwin, Li-Yan Tang, and A. G. Truscott, "Precision measurement for metastable helium atoms of the 413 nm tune-out wavelength at which the atomic polarizability vanishes," Phys. Rev. Lett. **115**, 043004 (2015).
[5] Felix Schmidt, Daniel Mayer, Michael Hohmann, Tobias Lausch, Farina Kindermann, and Artur Widera, "Precision measurement of the ^{87}Rb tune-out wavelength in the hyperfine ground state $F = 1$ at 790 nm," Phys. Rev. A **93**, 022507 (2016).
[6] M. S. Safronova, Carl J. Williams, and Charles W. Clark, "Relativistic many-body calculations of electric-dipole matrix elements, lifetimes, and polarizabilities in rubidium," Phys. Rev. A **69**, 022509 (2004).
[7] Bindiya Arora, M. S. Safronova, and Charles W. Clark, "Tune-out wavelengths of alkali-metal atoms and their applications," Phys. Rev. A **84**, 043401 (2011).
[8] Turker Topcu and Andrei Derevianko, "Tune-out wavelengths and landscape-modulated polarizabilities of alkali-metal Rydberg atoms in infrared optical lattices," Phys. Rev. A **88**, 053406 (2013).
[9] J. Mitroy and Li-Yan Tang, "Tune-out wavelengths for metastable helium," Phys. Rev. A **88**, 052515 (2013).
[10] Fam Le Kien, Philipp Schneeweiss, and Arno Rauschenbeutel, "Dynamical polarizability of atoms in arbitrary light fields: general theory and application to cesium," The European Physical Journal D **67**, 1–16 (2013).
[11] Jun Jiang and J. Mitroy, "Hyperfine effects on potassium tune-out wavelengths and polarizabilities," Phys. Rev. A **88**, 032505 (2013).
[12] Jun Jiang, Li-Yan Tang, and J. Mitroy, "Tune-out wavelengths for potassium," Phys. Rev. A **87**, 032518 (2013).
[13] Yongjun Cheng, Jun Jiang, and J. Mitroy, "Tune-out wavelengths for the alkaline-earth-metal atoms," Phys. Rev. A **88**, 022511 (2013).
[14] M. S. Safronova, Z. Zuhrianda, U. I. Safronova, and Charles W. Clark, "Extracting transition rates from zero-polarizability spectroscopy," Phys. Rev. A **92**, 040501 (2015).
[15] Wei-Wei Yu, Rong-Mei Yu, and Yong-Jun Cheng, "Tune-out wavelengths for the Rb atom," Chinese Physics Letters **32**, 123102 (2015).
[16] L. J. LeBlanc and J. H. Thywissen, "Species-specific optical lattices," Phys. Rev. A **75**, 053612 (2007).
[17] J. Catani, G. Barontini, G. Lamporesi, F. Rabatti, G. Thalhammer, F. Minardi, S. Stringari, and M. Inguscio, "Entropy exchange in a mixture of ultracold atoms," Phys. Rev. Lett. **103**, 140401 (2009).
[18] J. Catani, L. De Sarlo, G. Barontini, F. Minardi, and M. Inguscio, "Degenerate Bose-Bose mixture in a three-dimensional optical lattice," Phys. Rev. A **77**, 011603 (2008).
[19] Andrew J. Daley, Martin M. Boyd, Jun Ye, and Peter Zoller, "Quantum computing with alkaline-earth-metal atoms," Phys. Rev. Lett. **101**, 170504 (2008).
[20] Bryce Gadway, Daniel Pertot, Jeremy Reeves, and Dominik Schneble, "Probing an ultracold-atom crystal with matter waves," Nat Phys **8**, 544–549 (2012).
[21] Andreas Steffen, Andrea Alberti, Wolfgang Alt, Noomen Belmechri, Sebastian Hild, Michał Karski, Artur Widera, and Dieter Meschede, "Digital atom interferometer with single particle control on a discretized space-time geometry," Proceedings of the National Academy of Sciences **109**, 9770–9774 (2012).
[22] Raisa Trubko, James Greenberg, Michael T. St. Germaine, Maxwell D. Gregoire, William F. Holmgren, Ivan Hromada, and Alexander D. Cronin, "Atom interferometer gyroscope with spin-dependent phase shifts induced by light near a tune-out wavelength," Phys. Rev. Lett. **114**, 140404 (2015).
[23] R Chamakhi, H Ahlers, M Telmini, C Schubert, EM Rasel, and N Gaaloul, "Species-selective lattice launch for precision atom interferometry," New Journal of Physics **17**, 123002 (2015).
[24] David W Keith, Christopher R Ekstrom, Quentin A Turchette, and David E Pritchard, "An interferometer for atoms," Physical Review Letters **66**, 2693 (1991).
[25] P.R. Berman, *Atom Interferometry* (Academic Press, San Diego, 1997).
[26] Alexander D. Cronin, Jörg Schmiedmayer, and David E. Pritchard, "Optics and interferometry with atoms and molecules," Rev. Mod. Phys. **81**, 1051–1129 (2009).
[27] Philip R Bevington and D Keith Robinson, "Data reduction and error analysis," McGraw–Hill, New York (2003).
[28] Paul Hamilton, Matt Jaffe, Justin M Brown, Lothar Maisenbacher, Brian Estey, and Holger Müller, "Atom interferometry in an optical cavity," Physical review letters **114**, 100405 (2015).
[29] Raisa Trubko and Alexander D. Cronin, "Decoherence spectroscopy for atom interferometry," Atoms **4**, 25 (2016).
[30] V Bolpasi and W von Klitzing, "Double-pass tapered amplifier diode laser with an output power of 1W for an injection power of only 200 μW," Review of Scientific Instruments **81**, 113108 (2010).
[31] M. S. Safronova, Bindiya Arora, and Charles W. Clark, "Frequency-dependent polarizabilities of alkali-metal atoms from ultraviolet through infrared spectral regions," Phys. Rev. A **73**, 022505 (2006).
[32] M. S. Safronova, U. I. Safronova, and Charles W. Clark, "Magic wavelengths for optical cooling and trapping of potassium," Phys. Rev. A **87**, 052504 (2013).
[33] U. I. Safronova and M. S. Safronova, "High-accuracy calculation of energies, lifetimes, hyperfine constants, multipole polarizabilities, and blackbody radiation shift in ^{39}K," Phys. Rev. A **78**, 052504 (2008).
[34] W.R. Johnson, Dietmar Kolb, and K.-N. Huang, "Electric-dipole, quadrupole, and magnetic-dipole susceptibilities and shielding factors for closed-shell ions of the He, Ne, Ar, Ni (Cu+), Kr, Pb, and Xe isoelectronic sequences," Atomic Data and Nuclear Data Tables **28**, 333 – 340 (1983).
[35] D. K. Nandy, Yashpal Singh, B. P. Shah, and B. K. Sahoo, "Transition properties of a potassium atom," Phys. Rev. A **86**, 052517 (2012).
[36] U Volz and H Schmoranzer, "Precision lifetime measurements on alkali atoms and on helium by beam–gas–laser spectroscopy," Physica Scripta **1996**, 48 (1996).

[37] Maxwell D. Gregoire, Ivan Hromada, William F. Holmgren, Raisa Trubko, and Alexander D. Cronin, "Measurements of the ground-state polarizabilities of cs, rb, and k using atom interferometry," Phys. Rev. A **92**, 052513 (2015).

[38] Maxwell D. Gregoire, Nathan Brooks, Raisa Trubko, and Alexander D. Cronin, "Analysis of polarizability measurements made with atom interferometry," Atoms **4**, 21 (2016).

[39] H Wang, J Li, XT Wang, CJ Williams, PL Gould, and WC Stwalley, "Precise determination of the dipole matrix element and radiative lifetime of the K 39 4p state by photoassociative spectroscopy," Physical Review A **55**, R1569 (1997).

[40] St Falke, I Sherstov, E Tiemann, and Ch Lisdat, "The a 1sigma u+ state of k2 up to the dissociation limit." The Journal of chemical physics **125**, 224303–224303 (2006).

[41] Walter R Johnson, M Idrees, and J Sapirstein, "Second-order energies and third-order matrix elements of alkali-metal atoms," Physical Review A **35**, 3218 (1987).

[42] WR Johnson, ZW Liu, and J Sapirstein, "Transition rates for lithium-like ions, sodium-like ions, and neutral alkali-metal atoms," Atomic Data and Nuclear Data Tables **64**, 279–300 (1996).

[43] Robert Rafac and Carol Tanner, "Measurement of the ratio of the cesium D-line transition strengths," Phys. Rev. A **58**, 1087 (1998).

[44] E. Tiemann, H. Knöckel, and H. Richling, "Long-range interaction at the asymptote 3s+3 of na2," Zeitschrift für Physik D Atoms, Molecules and Clusters **37**, 323–332 (1996).

[45] K. M. Jones, P. S. Julienne, P. D. Lett, W. D. Phillips, E. Tiesinga, and C. J. Williams, "Measurement of the atomic na(3 p) lifetime and of retardation in the interaction between two atoms bound in a molecule," EPL (Europhysics Letters) **35**, 85 (1996).

[46] Jacek Migdalek and Yong-Ki Kim, "Core polarization and oscillator strength ratio anomaly in potassium, rubidium and caesium," Journal of Physics B: Atomic, Molecular and Optical Physics **31**, 1947 (1998).

[47] J MigdaŁek and E Banasińska, "Implicit and explicit treatment of valence-core electron exchange and core polarization in model potentials," Journal of Quantitative Spectroscopy and Radiative Transfer **39**, 409–414 (1988).

[48] J Migdalek and WE Baylis, "Local approximations for the exchange interaction between valence and core electrons," Physical Review A **22**, 22 (1980).

[49] A Corney and K Gardner, "A new method for determining f-values using stimulated electronic raman scattering in atomic vapours," Journal of Physics D: Applied Physics **11**, 1815 (1978).

[50] Winfried Hansen, "The application of polarisation-influenced Thomas-Fermi ion models to alkali-atom transitions," Journal of Physics B: Atomic and Molecular Physics **17**, 4833 (1984).

[51] Chou-Mou Huang and Charles C Wang, "Oscillator strength for principal series transitions to the high Rydberg states of potassium," Physical Review Letters **46**, 1195 (1981).

[52] M Szulkin and J Karwowski, "Core polarisation and relativistic effects in the alkali atoms," Journal of Physics B: Atomic and Molecular Physics **14**, 4729 (1981).

[53] GH Jeung, JP Malrieu, and JP Daudey, "Inclusion of core-valence correlation effects in pseudopotential calculations. I. alkali atoms and diatoms," The Journal of Chemical Physics **77**, 3571–3577 (1982).

[54] Inmaculada Martin and Carmen Barrientos, "Core-polarization effects in the alkali atoms: oscillator-strength calculations," Canadian Journal of Physics **64**, 867–871 (1986).

[55] Inmaculada Martin, Carmen Lavín, and Carmen Barrientos, "Systematic trends along the potassium sequence: Study of ns^2 S-mp^2 P 0 transitions," Canadian Journal of Physics **69**, 1273–1283 (1991).

[56] Carmen Barrientos and Inmaculada Martin, "Core-polarization effects in subordinate series of the alkali atoms," Canadian journal of physics **67**, 996–1001 (1989).

[57] Philip M Stone and Kim Yong-Ki, "Electron-impact cross sections for ground state to np excitations of sodium and potassium," Journal of Research of the National Institute of Standards and Technology **109**, 505 (2004).

[58] Jacek Karwowski and M Szulkin, "Relativistic calculations on the alkali atoms by a modified Hartree-Fock method," Journal of Physics B: Atomic and Molecular Physics **14**, 1915 (1981).

[59] E. Fermi, "Über das intensitätsverhältnis der dublettkomponenten der alkalien," Zeitschrift für Physik **59**, 680–686 (1930).

[60] Jacek Migdałek, "Model potential approach to core polarisation in SCF calculations," Physica Scripta **2002**, 47 (2002).

[61] J Migdalek and M Garmulewicz, "The relativistic ab initio model potential versus Dirac-Fock oscillator strengths for silver and gold isoelectronic sequences," Journal of Physics B: Atomic, Molecular and Optical Physics **33**, 1735 (2000).

[62] J Migdalek and M Wyrozumska, "Relativistic oscillator strengths for the Cs isoelectronic sequence and collapse of F and D orbitals," Journal of Quantitative Spectroscopy and Radiative Transfer **37**, 581–589 (1987).

[63] J Migdałek and WE Baylis, "Relativistic Hartree-Fock and model-potential ionization energies and oscillator strengths for transitions in the principal, sharp, and diffuse series of neutral rubidium and silver with allowance for core polarization," Canadian Journal of Physics **57**, 1708–1718 (1979).

[64] J Migdalek and WE Baylis, "Influence of atomic core polarisation on oscillator strengths for $^2S_{1/2}$ - $^2P_{1/2,3/2}$ and $^2P_{1/2,3/2}$ - $^2D_{3/2,5/2}$ transitions in Cu I, Ag I and Au I spectra," Journal of Physics B: Atomic and Molecular Physics **11**, L497 (1978).

[65] S. A. Blundell, J. Sapirstein, and W. R. Johnson, "High-accuracy calculation of parity nonconservation in cesium and implications for particle physics," Phys. Rev. D **45**, 1602–1623 (1992).